The following publication B. Liu et al., "A Novel Dual-Element Catheter for Improving Non-Uniform Rotational Distortion in Intravascular Ultrasound," in IEEE Transactions on Biomedical Engineering, vol. 70, no. 6, pp. 1768-1774, June 2023 is available at https://doi.org/10.1109/TBME.2022.3226955.

A Novel Dual-Element Catheter for Improving Non-Uniform Rotational Distortion in Intravascular Ultrasound

Baoqiang Liu, Min Su, Zhiqiang Zhang, Rong Liu, Lei Sun, Hairong Zheng, and Weibao Qiu

***Abstract*—For the early diagnosis of atherosclerosis and interventions, intravascular ultrasound (IVUS) is a valuable tool for intravascular luminal imaging. Compared with the array-based method, mechanically rotating IVUS catheters dominate the clinical applications because of their less complexity and better suitability for high-frequency ultrasound imaging. However, mechanically rotating catheters are suffering from non-uniform rotational distortion (NURD) which hinders accurate image acquisition. In this study, a dual-element imaging catheter is proposed, in which two elements with the same frequency and similar performance are assembled in a back-to-back arrangement. When the catheter encounters a NURD due to acute bending, the abnormal image of one element can be replaced by the normal image of the opposite element, thus eliminating the NURD in the reconstructed image. Moreover, two images can be obtained in one rotation and the imaging frame rate is doubled in the absence of NURD. The performance of the two elements was quantitatively assessed by a wire phantom. And the complementary imaging protocols were evaluated by a tissue phantom and *ex vivo* porcine vessel. The results show that the proposed strategy can be promising in clinical studies.**

***Index Terms*—Intravascular ultrasound (IVUS), Non-uniform rotation distortion (NURD), Dual-element catheter, Ultrasound imaging system.**

I. Introduction

ATHEROSCLEROSIS(AS) is an inflammatory disease featured by the development of a buildup of cholesterol, fibrous components, lipids, inflammatory cells, and monocytes in the walls of the arteries, which results in the narrowing and hardening of the arteries[1]. It is a major cause of acute ischemic lesions[2, 3]. Coronary angiography is commonly used for the diagnosis of atherosclerosis. X-rays and contrast agents are used to determine the location and extent of stenosis of the diseased vessel. However, it cannot present accurate information on vulnerable plaque and vessel wall structure, which are key parameters for assessing the severity of atherosclerotic lesions [4, 5].

Intravascular ultrasound (IVUS) is an invaluable tool in the diagnosis of atherosclerosis. It provides real-time, high-resolution, and valuable information about the coronary arteries, such as the degree of stenosis of the lumen, the morphology of the vessel wall, and the composition of the plaque. It has been applied to the quantification, characterization, and intervention guidance of atherosclerotic plaques, which has greatly enriched the understanding of atherosclerosis. At present, IVUS has been widely used as a mature technique for clinical diagnosis[1, 6, 7].

Two types of IVUS systems are now widely used in clinical practice: Solid State IVUS and Mechanical IVUS. The main difference between these two imaging strategies is the mode of ultrasonic wave transmitting and receiving. The solid-state IVUS consists of a 64 elements array transducer, uniformly arranged in a circle at the distal end of the catheter. The electronic system controls the transmission and reception of the elements through different time delays to obtain an anatomical image of the interior of the vessel[8, 9]. Due to the limitation of its small size, the imaging frequency is only up to 20 MHz of solid state IVUS, which is quite low for the IVUS application.

Mechanical IVUS is an ultrasound transducer with a single element installed at the distal end of a soft drive shaft. The proximal end of the soft drive shaft is attached to a motor that rotates to obtain real-time images of the tissue inside the vessel. Increasing the imaging frequency is an effective way to obtain higher resolution[10, 11]. Compared to the solid-state catheter, the mechanical rotation design is simpler and more suitable for high-frequency ultrasound imaging, thus enabling higher resolution and more widespread applications. However, excessive friction between the protective sheath and the drive shaft when the mechanical IVUS catheter passes through an extremely curved vessel segment often results in non-uniform rotational distortion(NURD) [12-14]. This is a characteristic of mechanical IVUS catheters that interferes with the accurate assessment of acutely curved coronary vessels [14-16].

Some image processing techniques take advantage of the similarity between frames, such as the analysis of IVUS images of different frames to track the tissue motion using cross-correlation [17], or using structural markers such as stents

Manuscript received July 26, 2022. This work was supported by the National Key R&D Program of China (2018YFA0701400, 2018YFA0902900, 2021ZD0200401), National Science Foundation Grants of China (62022086, 11874382, 11804358, and 81927808), Shenzhen Foundation Grant (JCYJ20200109114237902, SGDX2020110309400200, and ZDSYS201802061806314), CAS research projects (KFJ-PTXM-012, and 2011DP173015),China Postdoctoral Science Foundation (2017M622805), Natural Science Foundation of Guangdong Province (2020B1111130002 and 2020B1212060051), and Youth Innovation Promotion Association CAS 2018391.

B. Liu, M. Su, Z. Zhang, R. Liu, H. Zheng*, and W. Qiu* are with Paul C. Lauterbur Research Center for Biomedical Imaging, Shenzhen Institute of Advanced Technology, Chinese Academy of Sciences, Shenzhen 518055, China, are also with Shenzhen key laboratory of ultrasound imaging and therapy, Shenzhen 518055, China (*corresponding author, e-mail: hr.zheng@siat.ac.cn, and wb.qiu@siat.ac.cn).

M. Su, Lei Sun are with Department of Biomedical Engineering, The Hong Kong Polytechnic University, Hong Kong, China.

B. Liu, Z. Zhang, H. Zheng, W. Qiu are also with Shenzhen College of Advanced Technology, University of Chinese Academy of Sciences, Shenzhen 518055, China.

to help align the subsequently acquired data[18]. Frequency analysis of the IVUS vessel image texture was performed to evaluate the rotation angle and velocity of the transducer [19]. However, these cross-correlation techniques usually require highly correlated images. In addition, they are all computationally intensive and therefore difficult to correct in real-time [20, 21].

The catheter with a built-in micro-motor directly rotates the ultrasonic transducer or micro-reflector at the distal end, which can effectively improve the NURD to some extent. But its complexity is greatly increased, and the motor speed needs to be increased by increasing the current to improve the time resolution. The motor is in a narrow geometry, and the temperature increase is a concern for these methods[22-25]. The scheme of assembling two elements in one ultrasound catheter has been proposed, where the two elements are of different frequencies, one at high frequencies and the other at low frequencies, to use for super-harmonic imaging[26, 27] and to resolve the trade-off between resolution and penetration [28-32].

In this study, a dual-element imaging catheter was proposed to eliminate the NURD in IVUS, in which two elements with the same frequency and similar performance are assembled in a back-to-back arrangement. A dual-element IVUS imaging system is also designed and implemented. When the catheter has NURD due to acute bending, the abnormal image of one element can be replaced by the normal image of the opposite element. Furthermore, two images can be obtained in one rotation and the imaging frame rate is doubled in the absence of NURD. The wire phantom with five wires was used to estimate the imaging performance of both elements. Symmetry and consistency were validated. Complementary imaging reconstruction schemes were demonstrated with tissue-mimicking phantom and *ex vivo* porcine vessels. The experimental results suggest that the method proposed in this study is promising for the improvement of NURD artifacts.

II. Methods

A. Dual-Element Ultrasound Catheter Design and Fabrication

Considering the clinical use, the center frequency of two elements with the same size is designed to be 40 MHz[33]. Two identical frequency elements are assembled back-to-back in a copper housing to ensure that the dual-element catheter can be rotated in one rotation to obtain two frames with the same cross-section. Fig. 1 illustrates a schematic diagram of a dual-element ultrasound catheter with back-to-back assembly.

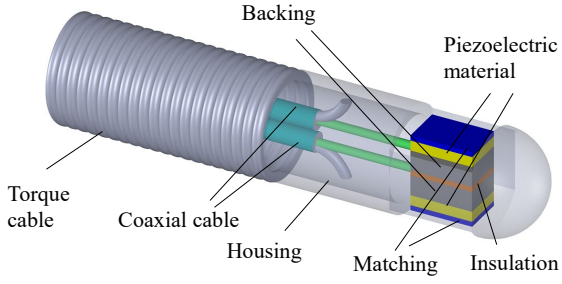

Fig. 1. Diagram of a dual-element ultrasound catheter assembled back-to-back.

For the choice of transducer material. PZT-5H (3203HD, CTS, Tianjin, China), a commonly used material, has a high electromechanical coupling coefficient, while the high Curie temperature gives it excellent stability and usually does not require repolarization after transducer assembly. [29, 30]. To optimize the acoustic impedance difference between the PZT-5H and the human body. Two matching layers were deposited in front of the PZT-5H. Table I presents the optimized parameters for the two-element catheter.

The fabrication of two elements in the catheter is as follows: First, a PZT-5H (3203HD, CTS, Tianjin, China) ceramic sample was glued on a sapphire substrate and was lapped to a thickness of 50 μm using a high-precision lapping and polishing systems (EJ-380IN-D, Engis-Japan Co., Ltd., Yokohama, Japan). The Cr/Au layer was then sputtered as an electrode on both sides of the ceramic samples. A mixture of 2-3 μm silver particles (Sigma-Aldrich Inc., St. Louis, MO, USA) and Insulcast 502 (ITW Polymers Coatings North America, Montgomeryville, PA, USA) was mixed well. It was then cast on one electrode surface and used as the first matching layer. The first matching layer was then lapped down to 10μm. Conductive epoxy resin (E-solder 3022, Von Roll Isola, New Haven, CT) was cured on the other side of the sample to act as a backing. The sample was then diced into small elements with an aperture of 0.4 × 0.6 mm^2. Two elements were attached back-to-back with insulating epoxy resin and assembled into a copper housing (OD: 0.96 mm). E-Solder was also used to connect the signal lines of two coaxial cables to the backing layer of the elements respectively. The two coaxial cables were then installed in a flexible drive shaft (OD: 0.86 mm). The ground of two of the coaxial cables was connected to the copper housing via an E-Solder. This was followed by sputtering of the Cr/Au layer on the copper housing to ensure the adequate connection of the GND. Finally, a layer of parylene was vapor-deposited as the second matching layer.

B. Characterization of The Dual-Element Catheter

The pulse-echo response of both elements (element A and element B) was tested by placing the catheter in a deionized water bath at room temperature. A strong reflector (quartz plate) was placed in the water in front of the transducer as a target. A pulser/receiver (DPR500, JSR Ultrasonics, Pittsford, NY) emitted a 143 V unipolar negative pulse to excite the transducer. The energy of each pulse was controlled at 3μJ. The gain of the echo signal was set to 14 dB. The output of the pulser/receiver was input to a digital oscilloscope (DPO4104, Tektronix, Inc, Beaverton, OR, USA) with a sampling rate of 5 GS/s and bandwidth of 1 GHz for digital processing. The center

TABLE I
Design Parameters of The Catheter

Number of element	2
Center frequency (MHz)	40
Aperture size (mm)	0.4×0.6
Piezo - material	PZT-5H
1st Matching layer material	Ag/epoxy
2st Matching layer material	Parylene
Backing layer material	E-solder

frequency of the transducer and the -6 dB bandwidth (BW) were calculated based on the data obtained from the oscilloscope. A combined mechanical and electrical crosstalk between two elements of the catheter was tested. During the crosstalk testing, the function generator (DG4102, RIGOL Technologies, Beijing, China) was set to burst mode to generate a 40MHz, 15-cycle, 10-Vpp sine wave to excite one of the elements. The voltage of the other element was measured by an oscilloscope (Wavepro715Zi, Teledyne LeCroy, Chestnut Ridge, NY).

C. Dual-Channel Real-Time Imaging System

A dual-channel real-time ultrasound imaging system was designed and fabricated as presented in Fig. 2. It included a dual-element catheter, rotating device, dual-channel imaging platform, and PC, where the dual-channel imaging platform was a 12-layer PCB board containing two sets of pulser/receivers. The power supply unit could generate positive and negative high voltage to support bipolar pulse excitation. The pulse excitation scheme was implemented using a high voltage, high current output, and low threshold metal oxide semiconductor field effect transistor (MOSFET). The MOSFET driver was controlled by an FPGA (Cyclone-V 5CGTFD7D5F31C7, Intel Corporation, Santa Clara, California) to adjust the excitation pulse duration and spectral characteristics. The dual-element catheter was connected to a signal coupling device which was fixed to a rotating motor, thus enabling signal coupling during the 360° rotation of the catheter. In the receiver section, the echo signal passed through a transmit/receive switch (TRSW) before entering a high-pass filter for filtering out low frequency noise. A two-stage amplifier was then used, which had a very low noise figure of 1.7 and a total system gain of 52.6 dB. A single-ended to differential circuit was designed behind the low-noise amplifier. A two-channel high-speed 14-bit ADC (AD6674, Analog Devices, Norwood, MA) was used to digitize the ultrasound signal with a sample rate of 500 MSPS. Also to prevent high frequency noise from being mixed with the useful ultrasound signal. A fifth-order low-pass filter was designed in front of the ADC. The digital signals were transferred to the FPGA via the JESD204B interface. The echo data were digitally processed in the FPGA by digital filters, Hilbert transforms, and envelope detection. The USB 3.0 interface served as the interaction channel between the PC and the imaging platform. The imaging software could send parameters to the imaging platform to control the data acquisition and also implement a real-time display of the dual channel data.

D. Evaluation of Wire Phantom

Five 10 μm diameter tungsten wires (Goodfellow Ltd, Cambridge, UK) were fixed on concentric circles with different radii to form a wire phantom. This was used to estimate the spatial resolution of the transducer, as well as the symmetry and consistency of the dual-element catheter assembly. Place the wire phantom in a sink filled with deionized water, then the dual-element catheter was put in the centers of the concentric circles of the wire phantom. The proximal end of the catheter was attached to a rotating device where a motor drove the catheter to rotate at a speed of 20 r.p.m. Each of these frames had 500 scan lines. The data was saved and the wire phantom images were then displayed and analyzed using Matlab software.

E. Evaluation of Tissue Phantom

Fig. 3 shows an agar-based tissue phantom to assess the effect of the dual-element catheter on the correction of NURD images. Two hypoechoic holes of different diameters (2 mm, and 3 mm) were made, respectively, with the 2 mm hole used to evaluate the integrity of the tissue information after image correction. Since the imaging holes of the tissue-mimicking phantom were regularly circular, so *ex vivo* porcine vessels with irregular lumen were chosen to further evaluate the effect of a dual-element catheter on the correction of NURD images.

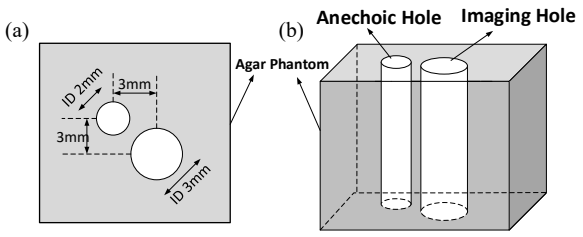

Fig. 3. Illustration of the tissue-mimicking phantom: (a) top view and (b) 3D view.

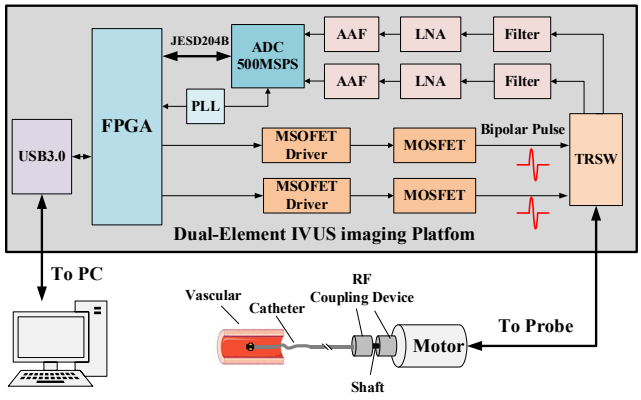

Fig. 2. Schematic diagram of the dual-channel real-time IVUS imaging system.

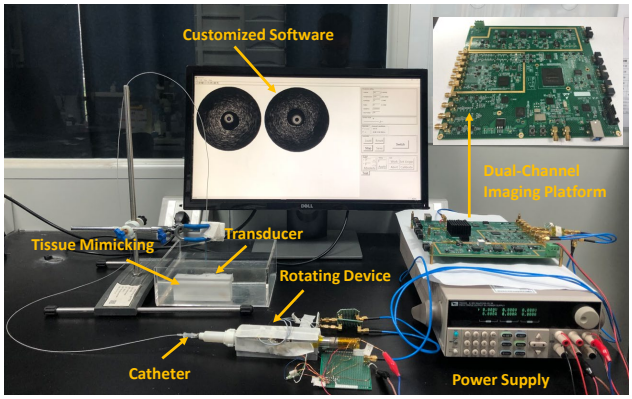

Fig. 4. Prototype of the customized dual-element IVUS system, including a rotating device, a catheter, a power supply, a tissue mimicking, a customized software and a dual-element imaging platform.

The rotation speed of the catheter is 20Hz. For each rotation of the catheter, the system obtained two frames simultaneously. Rotating one of the frames by 180° will give the same image as the other frame. Therefore, when a NURD appeared in one frame, the same NURD appeared on the symmetrical side of the other frame.

F. Image Reconstruction

Since a frame of image consists of 500 A-lines, we replace the data between the first and 250th A-lines where the NURD appears using the normal tissue image (~250 A-lines) acquired by the opposite element. The three adjacent lines were smoothed using Gaussian filter at the location where the images were stitched. A more complete image was reconstructed by extracting the normal tissue information from the two frames.

III. RESULTS

A. Performance of the Electrical System

Fig. 4 shows a picture of the customized dual-element IVUS real-time imaging system. The system's receiving channel has a bandwidth of 20-75 MHz. The dual-channel pulse generator circuit can generate a bipolar pulse with a center frequency of 44.9MHz, a peak-to-peak of 94Vpp, and a -6dB bandwidth of 141%. The frequency range covers the application of the dual-element probe. The JESD204B is used as a high-speed data transfer interface between the ADC and the FPGA at rates up to 12.5 Gbps. USB3.0 transfer rates are greater than 100 MB/S. This achieves simultaneous acquisition and display of dual channel data.

B. Performance of The Dual-Element Catheter

The picture of the dual-element imaging catheter and transducer is illustrated in Fig. 5 (a). Fig. 5(b-c) gives the measured pulse-echo response of two elements. The center frequency of element A and element B was 40.4 MHz and 41.1 MHz respectively. 67% and 63.3% of the -6 dB bandwidth of the two elements were obtained respectively. The crosstalk between the two elements is -68 dB. The performance of the two elements was nearly the same, which met the desired requirements.

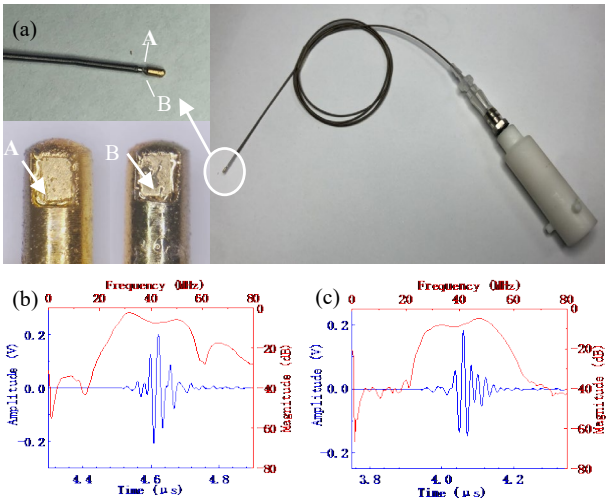

Fig. 5. Images of the catheter and Pulse-echo Results. (a) Pictures of dual-element IVUS imaging catheter, (b) pulse-echo result for element A (40.4 MHz), (c) pulse-echo result for element B (41.1 MHz).

C. Wire Phantom

The wire phantom images acquired by the dual-element IVUS catheter are illustrated in Fig. 6(a) and (b). The echo amplitude of the wire phantom was close in both images. This demonstrated the consistency of the imaging of both elements. In addition, the average position of the five wires in Fig. 6(a) appeared to be between 21° and 31°. In Figure 6(b) the average position of the five wires appeared to be between 198° and 208°. In the circular diagram, the angular difference of the wire Phantom was close to 180°. This proved that the symmetry of the two elements assemblies also met the design requirement. Resolutions for both elements are illustrated in Fig. 6(c-f). The axial resolutions of the elements A and B were 30.7 μm and 33.8 μm respectively, corresponding to lateral resolutions of 167.3 μm and 184.6 μm respectively. The SNRs for the image acquired by element A and element B were 25.2 and 23.4 dB, respectively.

D. Tissue Imaging

Fig. 7 (a-c) shows the images of the tissue-mimicking phantom. The inner lumen of the imaging is regularly circular. To facilitate comparison, the first lines of the two frames are placed symmetrically at 180°. The image data are shown in a

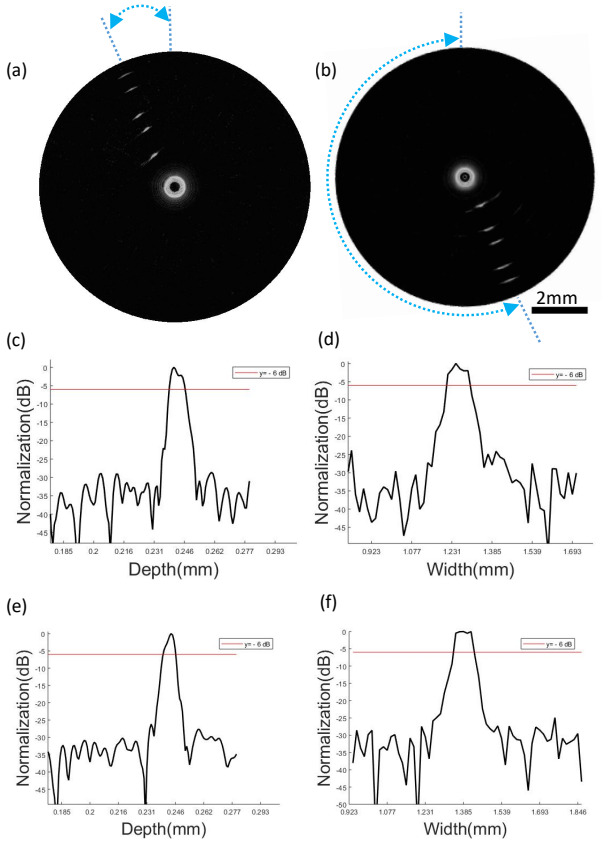

Fig. 6. Wire phantom images and resolution results. (a) image acquired by element A, (b) image acquired by element B. Resolution of the element A and B: (c, e) axial resolution , (d, f) lateral resolution. Dynamic range: 35dB.

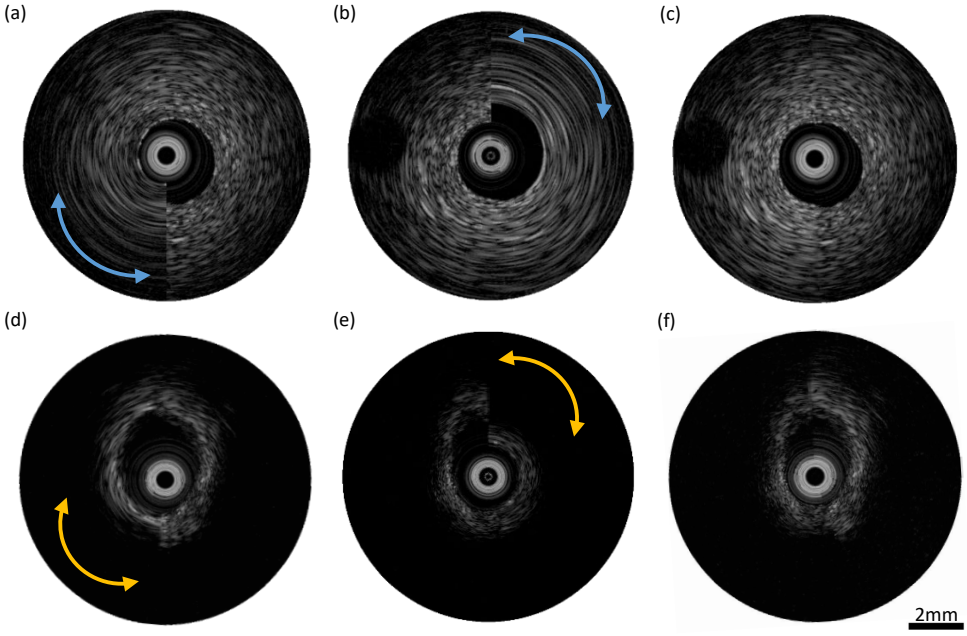

Fig. 7. Tissue images of the dual-element catheter. Tissue-mimicking phantom images.(a) NURD ultrasound image of element A, (b) NURD ultrasound image of element B, (c) Reconstructed image after extracting half of the data from each of the A and B images. *Ex vivo* porcine vessels images. (d) NURD ultrasound image of element A, (e) NURD ultrasound image of element B, (f) Reconstructed image after extracting half of the data from each of the A and B images. Dynamic range: 35dB.

counterclockwise direction. Fig. 7(a) and (b) present the NURD images of elements A and B respectively. This image was achieved by bending the catheter acutely. In Fig. 7 (a), the right part of the image is normal, but the left part has NURD (shown by the blue arrow) and the information about the hole is lost. Meanwhile, the right part of Fig. 7(b) has NURD (shown by the blue arrow), but the left part is normal and a hypoechoic hole can be seen. As shown in Fig. 7 (c), we extracted half of the normal tissue from each of the two images in Fig. 7(a) and (b), and reconstructed them into a complete frame. The position of the image stitching was smoothed using a Gaussian filter.

Fig. 7(d-f) shows an image of an *ex vivo* porcine vessel. The lumen of the imaging is irregularly rounded. Fig. 7(d) and (e) show the NURD images of elements A and B, respectively. This image was also achieved by bending the catheter acutely. The NURD of element A appeared at the bottom left of the image (yellow arrowed area) and the right part of the image was normal. The NURD of element B appeared at the top right of the image (yellow arrow area) but the image on its left side was normal. A complete frame of the vascular image was reconstructed by extracting the right part of the image of element A and the left part of the image of element B, respectively. This is shown in Fig. 7(f), which indicates the NURD has been improved.

IV. Discussion

For the early diagnosis of atherosclerosis and interventions, intravascular ultrasound (IVUS) is a valuable tool for intravascular luminal imaging. Compared to solid-state catheters, mechanical rotational designs are less complex and more suitable for high-frequency imaging, achieving higher resolution, and thus gaining more popularity. However, mechanically rotating catheters are prone to NURD artifacts. NURD is a motion artifact specific to mechanically rotating catheters. It will result in significant limitations for quantitative analysis of the vessel lumen.

In catheter-based imaging systems such as IVUS or OCT, there have been previous studies to improve NURD through correlation algorithms[17, 19], or the use of structural markers such as stents to help align subsequently acquired data[18]. These techniques often require highly correlated images. This study presents a novel dual-element IVUS catheter with a back-to-back transducer assembly. The center frequencies and apertures of the two components are designed to be identical. A dual-channel real-time imaging system was also built in this study, in which an imaging platform was designed and fabricated to enable simultaneous dual-channel transceivers. The complementarity and symmetry of the two elements were verified by wire phantom imaging. The axial resolutions of the two elements are 30.7 μm and 33.8 μm respectively, corresponding to lateral resolutions of 167.3 μm and 184.6 μm respectively. The complementary imaging effect of the two elements was verified with tissue-mimicking phantom and *ex vivo* porcine vessel, respectively.

Due to the imaging holes of the tissue-mimicking being regular circles and the tissue composition being homogeneous, the image reconstruction is better than that of the *ex vivo* vessels. No obvious signs of stitching are seen. Splice marks are evident in the *ex vivo* vessels, but this does not affect the reconstruction and observation of the lost tissue. Furthermore, it is not easy to fabricate the two elements catheter. Both elements need to be assembled in the same way inside the housing. At the same time, the assembly of the housing and the soft drive shaft must be kept in line. Typically, NURD of IVUS catheter occurs at an angle of less than 180 degrees. This can distort both transducers in a situation where the drive shaft is

stuck and cannot rotate. The proposed method does not work in this extreme case. Currently, we have been able to acquire images from both channels simultaneously and processed the data offline. The NURD can be automatically detected by analyzing the correlation of consecutive A-lines. For example, for a 360-degree image, there are 500 A-lines, and for a 10-degree image angle, there are approximately 14 A-lines. Correlation analysis of the 14 consecutive A-lines can be used to determine the presence or absence of NURD. Of course, the number of data lines detected at one time is appropriately adjusted according to the data processing capacity of the system.

V. Conclusion

A dual-element imaging catheter is proposed in this study, in which two elements with the same frequency and similar performance are assembled in a back-to-back arrangement. The center frequency and -6dB bandwidth of the two elements are 40.4 MHz, 67%, and 41.1 MHz, 63.3% respectively. The catheter can obtain two imaging frames in one rotation. When the catheter encounters a NURD due to acute bending, the abnormal image of one element can be replaced by the normal image of the opposite element. Therefore, the NURD can be eliminated by the implemented dual-element catheter for IVUS applications.

VI. References

[1] C. Peng *et al.*, "Recent Advances in Transducers for Intravascular Ultrasound (IVUS) Imaging," *Sensors,* vol. 21, no. 10, pp. 3540, 2021.

[2] J. Narula, and H. W. Strauss, "Imaging of unstable atherosclerotic lesions," *Eur J Nucl Med Mol Imaging,* vol. 32, no. 1, pp. 1-5, Jan, 2005.

[3] C. Weber, and H. Noels, "Atherosclerosis: current pathogenesis and therapeutic options," *Nat Med,* vol. 17, no. 11, pp. 1410-22, Nov 7, 2011.

[4] P. de Feyter *et al.*, "Quantitative coronary angiography to measure progression and regression of coronary atherosclerosis. Value, limitations, and implications for clinical trials," *Circulation (Baltimore),* vol. 84, no. 1, pp. 412-423, Jan, 1991.

[5] B. N. Potkin *et al.*, "Coronary artery imaging with intravascular high-frequency ultrasound," *Circulation,* vol. 81, no. 5, pp. 1575-1585, 1990.

[6] F. Deleaval *et al.*, "The intravascular ultrasound elasticity-palpography technique revisited: a reliable tool for the in vivo detection of vulnerable coronary atherosclerotic plaques," *Ultrasound in medicine & biology,* vol. 39, no. 8, pp. 1469-1481, 2013.

[7] X. Li *et al.*, "Micromachined PIN-PMN-PT crystal composite transducer for high-frequency intravascular ultrasound (IVUS) imaging," *IEEE transactions on ultrasonics, ferroelectrics, and frequency control,* vol. 61, no. 7, pp. 1171-1178, 2014.

[8] H.-B. Park *et al.*, "IVUS Artifacts and Image Control," *Coronary Imaging and Physiology*, M.-K. Hong, ed., pp. 9-17, Singapore: Springer Singapore, 2018.

[9] T. Teo, "Intravascular ultrasound (IVUS) — Technologies and applications." pp. 760-769.

[10] C. C. Huang *et al.*, "40 MHz high-frequency ultrafast ultrasound imaging," *Med Phys,* vol. 44, no. 6, pp. 2185-2195, Jun, 2017.

[11] T. Y. Liu *et al.*, "A study of the adult zebrafish ventricular function by retrospective doppler-gated ultrahigh-frame-rate echocardiography," *IEEE Transactions on Ultrasonics, Ferroelectrics, and Frequency Control,* vol. 60, no. 9, pp. 1827-1837, 2013.

[12] S. Hou *et al.*, "A Novel Distal Micromotor-Based Side-Looking Intravascular Ultrasound Transducer," *IEEE Transactions on Ultrasonics, Ferroelectrics, and Frequency Control,* vol. 69, no. 1, pp. 283-290, 2022.

[13] M. C. McDaniel *et al.*, "Contemporary Clinical Applications of Coronary Intravascular Ultrasound," *JACC: Cardiovascular Interventions,* vol. 4, no. 11, pp. 1155-1167, 2011/11/01/, 2011.

[14] Y. Kawase *et al.*, "Comparison of nonuniform rotational distortion between mechanical IVUS and OCT using a phantom model," *Ultrasound in Medicine & Biology,* vol. 33, no. 1, pp. 67-73, 2007/01/01/, 2007.

[15] B. J. Kimura *et al.*, "Distortion of intravascular ultrasound images because of nonuniform angular velocity of mechanical-type transducers," *American Heart Journal,* vol. 132, no. 2, Part 1, pp. 328-336, 1996/08/01/, 1996.

[16] P. P. Kearney *et al.*, "A study of the quantitative and qualitative impact of catheter shaft angulation in a mechanical intravascular ultrasound system," *Ultrasound in Medicine & Biology,* vol. 23, no. 1, pp. 87-93, 1997/01/01/, 1997.

[17] C. Gatta *et al.*, "Fast rigid registration of vascular structures in IVUS sequences," *IEEE transactions on information technology in biomedicine : a publication of the IEEE Engineering in Medicine and Biology Society,* vol. 13, no. 6, pp. 1006-1011, 2009/11//, 2009.

[18] G. Ughi *et al.*, "Automatic three-dimensional registration of intravascular optical coherence tomography images," *Journal of Biomedical Optics,* vol. 17, no. 2, pp. 026005, 2012.

[19] S. Shashidhar, *NONUNIFORM ROTATIONAL DISTORTION (NURD) REDUCTION*,to BOSTON SCIENTIFIC LIMITED, 2003.

[20] B. E. Uribe-Patarroyo N Fau - Bouma, and B. E. Bouma, "Rotational distortion correction in endoscopic optical coherence tomography based on speckle decorrelation," no. 1539-4794 (Electronic), 2015.

[21] O. O. Ahsen *et al.*, "Correction of rotational distortion for catheter-based en face OCT and OCT angiography," *Optics Letters,* vol. 39, no. 20, pp. 5973-5976, 2014/10/15, 2014.

[22] M. Salimuzzaman *et al.*, "Blood Vessel Visualization Using a Micromotor Type Intravascular Ultrasound Endoscope," *Japanese Journal of Applied Physics,* vol. 36, no. Part 1, No. 5B, pp. 3250-3254, 1997/05/30, 1997.

[23] T. Wang *et al.*, "Development of a high-speed synchronous micro motor and its application in intravascular imaging," *Sensors and Actuators A: Physical,* vol. 218, pp. 60-68, 2014/10/01/, 2014.

[24] J. Peng *et al.*, "A Novel Synchronous Micro Motor for Intravascular Ultrasound Imaging," *IEEE Transactions on Biomedical Engineering,* vol. 66, no. 3, pp. 802-809, 2019.

[25] P. R. Herz *et al.*, "Micromotor endoscope catheter for in vivo, ultrahigh-resolution optical coherence tomography," *Optics Letters,* vol. 29, no. 19, pp. 2261-2263, 2004/10/01, 2004.

[26] J. Ma *et al.*, "A preliminary engineering design of intravascular dual-frequency transducers for contrast-enhanced acoustic angiography and molecular imaging," *IEEE Transactions on Ultrasonics, Ferroelectrics, and Frequency Control,* vol. 61, no. 5, pp. 870-880, 2014.

[27] Z. Wang *et al.*, "Real-time ultrasound angiography using superharmonic dual-frequency (2.25MHz/30MHz) cylindrical array: In vitro study," *Ultrasonics,* vol. 82, pp. 298-303, Jan, 2018.

[28] W. Qiu *et al.*, "A novel dual-frequency imaging method for intravascular ultrasound applications," *Ultrasonics,* vol. 57, pp. 31-35, 2015/03/01/, 2015.

[29] T. Ma *et al.*, "Multi-frequency intravascular ultrasound (IVUS) imaging," *IEEE transactions on ultrasonics, ferroelectrics, and frequency control,* vol. 62, no. 1, pp. 97-107, 2015.

[30] C. E. Munding *et al.*, "Development of a 3 French Dual-Frequency Intravascular Ultrasound Catheter," *Ultrasound Med Biol,* vol. 44, no. 1, pp. 251-266, Jan, 2018.

[31] M. Su *et al.*, "Cable-Shared Dual-Frequency Catheter for Intravascular Ultrasound," *IEEE Transactions on Ultrasonics, Ferroelectrics, and Frequency Control,* vol. 66, no. 5, pp. 849-856, 2019.

[32] Y. Sangpil *et al.*, "Dual-element needle transducer for intravascular ultrasound imaging," *Journal of Medical Imaging,* vol. 2, no. 2, pp. 1-9, 4/1, 2015.

[33] C. C. Huang, "High-frequency attenuation and backscatter measurements of rat blood between 30 and 60 MHz," *Phys Med Biol,* vol. 55, no. 19, pp. 5801-15, Oct 7, 2010.